Fe(III)-Pt(II) Oxide-Co-Sensitized Brookite TiO_2 Nanorods for Photocatalytic Degradation of Acetaldehyde under Visible Light

Yu Cao[1,4,#], Shi Nee Lou[2,#], Sicong Wang[4], Hui Yang[3], Qitao Zhang[5*], Chengyin Wang[4*], Naoya Murakami[1*], Teruhisa Ohno[1*]

1. Department of Applied Chemistry Section, Faculty of Engineering, Kyushu Institute of Technology, 1-1 Sensui-cho Tobata-ku, Kitakyushu, Fukuoka, 804-8550, Japan.

2. Division of Environmental Science and Engineering, Pohang University of Science and Technology (POSTECH), 77, Cheongam-ro, Nam-gu, Pohang-si, Gyeongsangbuk-do, 37673, Republic of Korea

3. School of Chemistry and Chemical Engineering, Yangzhou University, 180 Si-Wang-Ting Road, Yangzhou 225002, China.

4. College of Chemistry and Chemical Engineering, Jiangsu Key Laboratory of Environmental Engineering and Monitoring, Yangzhou University, 180 Si-Wang-Ting Road, Yangzhou, 225002, China.

5. International Collaborative Laboratory of 2D Materials for Optoelectronics Science and Technology of Ministry of Education, Institute of Microscale Optoelectronics, Shenzhen University, Shenzhen 518060, China

# These authors contributed equally.

Email addresses:

Qitao Zhang: qitao-zhang@szu.edu.cn

Chengyin Wang: wangcy@yzu.edu.cn

Naoya Murakami: murakami@life.kyutech.ac.jp

Teruhisa Ohno: tohno@che.kyutech.ac.jp

Highlights

- Surface-controlled brookite TiO_2 nanorods were obtained by hydrothermal synthesis with TALH and urea
- Pt metal and oxide sensitizers modified on brookite TiO_2 nanorod surfaces were investigated for acetaldehyde degradation under visible light
- Pt(II) oxide-sensitized brookite TiO_2 (Pt(II)/TiO_2) showed significantly higher photocatalytic activity but lower stability for acetaldehyde degradation compared to Pt(IV) oxide or Pt(0)-sensitized brookite TiO_2
- Surface coating of an Fe(III) oxide sensitizer layer on Pt(II)/TiO_2 nanorod surface (Fe(III)-Pt(II)/TiO_2) enhanced both the activity and stability of Pt(II)/TiO_2 for acetaldehyde degradation under visible light
- Mechanistic insights into the electron transfer mechanisms within Fe(III)-Pt(II)/TiO_2 and Pt(II)/ TiO_2 were unraveled using *in situ* double beam photoacoustic spectroscopy (DB-PAS) and supported by DFT modelling

Abstract

Platinum is widely investigated as co-catalysts for photocatalytic degradation of volatile organic compounds but studies seldom focus on their visible light sensitizing properties. Herein, Pt sensitizers of different oxidation states (0, II, IV) were modified on brookite TiO_2 nanorods and investigated for acetaldehyde degradation under visible light. Pt(II) oxide/TiO_2 showed the best photocatalytic activity but its stability was compromised by its self-oxidation to Pt(IV) during photo-oxidation reaction. Surface modification of an Fe(III) oxide thin film sensitizer layer around the Pt(II) oxide sensitizer was found to enhance both the stability and activity of Pt(II) oxide/TiO_2. *In situ* double beam photoacoustic spectroscopy (DB-PAS) supported by DFT modelling showed the rapid injection of photoexcited electrons from Fe(III) oxide to Pt(II) oxide promote the stability of Pt(II) oxide, leading to enhanced performance. The findings provide guidance for the rational design of visible light-active metal oxide sensitizers for oxidative removal of indoor air pollutants.

Keywords

TiO_2, indoor VOCs degradation, visible light sensitizers, Pt sensitizers, Fe sensitizers

1. Introduction

In our contemporary society, people spend on average 80% of their time indoors. Indoor air quality has therefore become an important issue for human health.[1] Volatile organic compounds (VOCs) are notable indoor air pollutants as well as other compounds such as NO_x, SO_2, ozone and particulate matters.[2-5] Indoor VOCs such as aldehydes, amines and aromatic compounds can be emitted from indoor sources and activities including cooking, secondhand smoke, cleaning, consumer products, home furnishings and building materials. Moreover, in recent years, indoor air pollutants have been increasingly associated with sick building syndrome (SBS).[6-9]

Photocatalytic systems that can decompose VOCs to CO_2 are promising methods for removing indoor VOCs. Photocatalytic degradation of VOCs with various materials such as TiO_2, C_3N_4, WO_3, SnO_2 and $BiVO_4$ has been demonstrated.[10-13] Although photocatalytic systems can remove VOCs by photooxidative destruction, the removal efficiency is very low under normal indoor light conditions due to the lack of adequate energetic photons. The development of photo-conversion materials that can utilize visible light photons at the maximum capacity should enable effective removal of indoor air pollutants under indoor light conditions.

Metallic Pt (i.e., Pt(0)) is widely used as a cocatalyst for various photocatalytic reactions including hydrogen evolution reaction and NO_x and CO_2 reduction reaction owing to its ability to promote interfacial charge separation as well as its favorable catalytic properties.[14-16] Recently, Pt in its 2+ and 4+ oxidation state, (Pt(II) and Pt(IV)), respectively, have also been reported to be visible light active catalysts (or sensitizers) for NO_x oxidation[17, 18], organic compounds degradation[19, 20] and hydrogen evolution reaction.[21] However, it is unclear if Pt in its metallic form or oxide form is the most active form of visible light sensitizer for photocatalytic degradation of VOCs.

TiO_2 is a non-toxic and relatively cheap photoconversion material. TiO_2 exists in three crystalline structures: anatase, rutile and brookite phases. Most photocatalytic studies have focused on the anatase and rutile phases of TiO_2 due to their relatively high thermal stability and ease of preparation.[22, 23] Although brookite TiO_2 is not as commonly used as that of anatase or rutile TiO_2 owing to its metastability, brookite TiO_2 has shown high photocatalytic activities for the degradation of various recalcitrant pollutants.[24, 25] W.-K. Li et al. found the exposed {210} facet of brookite TiO_2 is more reactive than the {101} facet of anatase TiO_2, which is thus beneficial for improving photocatalytic reactions.[26] Brookite TiO_2 also showed higher surface affinity for O_2 adsorption than anatase TiO_2 in oxygen reduction reaction to produce H_2O_2.[27] Moreover, brookite TiO_2 was demonstrated to oxidize propanone to CO_2 and H_2O much faster than

anatase TiO_2. Brookite TiO_2 also exhibited higher areal photocatalytic activity for RhB degradation than rutile TiO_2 and anatase TiO_2.[28, 29] These observations suggest brookite TiO_2 is a promising photoconversion material for solving environmental issues.

In this study, brookite TiO_2 nanorods with well-defined {210} and {111} facets were synthesized by a hydrothermal process utilizing TALH and urea as precursors. Acetaldehyde was used as a representative indoor VOC. Pt(0) metal sensitizer and Pt(II) and Pt(IV) oxide sensitizers were incorporated on the surfaces of the brookite TiO_2 nanorods by a photodeposition method or a chemisorption method.

Our results show Pt(II) oxide-sensitized brookite TiO_2 (Pt(II)/TiO_2) exhibits higher photocatalytic activity than that of Pt(0)/TiO_2 or Pt(IV) oxide/TiO_2 for acetaldehyde degradation under visible light. However, the photocatalytic activity of Pt(II)/TiO_2 is hindered by the low stability of Pt(II) oxide, which readily oxidizes to Pt(IV) oxide with increased reaction time. We then developed strategies to overcome the stability issues of a Pt(II) oxide sensitizer. We found a simultaneous photodeposition of Pt(IV) ions and Fe(II) cations onto brookite TiO_2 nanorods resulted in selective formation of island-like PtO and $Pt(OH)_2$ nanoclusters on the {210} facet of brookite TiO_2 nanorods with a film-like Fe(III) oxide layer covering the entire surface of the Pt(II)/TiO_2 nanorods. The Fe(III) oxide thin film layer not only serves as a protective layer preventing Pt(II) oxide from ambient oxidation but also acts as a visible light sensitizer. The Fe(III)/Pt(II)-oxide-co-sensitized brookite TiO_2 nanorods (Fe(III)-Pt(II)/TiO_2) show dramatic enhancements in both activity and stability for acetaldehyde degradation under visible light illumination. The electron transfer mechanisms leading to the enhanced photocatalytic performance were unraveled by *in situ* double beam photoacoustic spectroscopy (DB-PAS), XPS and UV-Vis spectroscopy and supported by density functional theorem (DFT) computational modeling.

2. Results and Discussion

2.1 Surface and Structural Properties

Scheme 1 shows the material flowchart leading to the synthesis of metallic Pt-sensitized brookite TiO_2 nanorods (Pt(0)/TiO_2), Pt(II)-sensitized brookite TiO_2 nanorods (Pt(II)/TiO_2) and Pt(IV)-sensitized brookite TiO_2 nanorods (Pt(VI)/TiO_2). In brief, Pt(0)/TiO_2 is prepared by photodeposition of Pt^{4+} ions onto TiO_2 nanorod surfaces using an aqueous solution containing chloroplatinic acid ($H_2Pt(IV)Cl_6$) and ethanol as the hole scavenger. Pt(II) and Pt(IV)-sensitized TiO_2 are synthesized by chemisorption of Pt(II)

and Pt(IV) ions under dark conditions from an aqueous solution of potassium tetrachloroplatinate ($K_2Pt(II)Cl_4$) or $H_2Pt(IV)Cl_6$.

Fig. S1 of Supporting Information (SI) show the high-resolution transmission electron microscopy (HRTEM) images and a selected area electron diffraction (SAED) pattern of a pure brookite TiO_2 nanorod sample. The HRTEM images (Fig. S1a-c, SI) show the brookite TiO_2 rods have a prismatic morphology with tapered ends and smooth surfaces. The length and width of the brookite TiO_2 nanorods are ~150.0 nm and 26.7 nm, respectively. In addition, the lattice plane imaging (Fig. S1c, SI) shows the brookite TiO_2 nanorods possess a well-defined {210} body facet and a {111} tapered end facet.[30, 31] Moreover, the single bright spots of an SAED pattern of a brookite TiO_2 nanorod, as shown in Fig. S1d (SI), indicate the brookite TiO_2 nanorods are single crystalline brookite TiO_2. Fig. S2 (SI) shows the XRD spectra of the as-prepared brookite TiO_2 sample. The XRD spectra show only diffraction peaks of brookite phase TiO_2 (JCPDS NO. 29-1360). No diffraction peak associated with other phase (anatase or rutile phase) of TiO_2 was observed, indicating the as-prepared TiO_2 are pure brookite-phase TiO_2[32]. The high purity of the as-prepared brookite TiO_2 was also collaborated by a Raman spectrum, as shown in Fig. S3 (SI).[33]

Fig. S4a-c (SI) show the Pt 4f XPS spectra for $Pt(0)/TiO_2$, $Pt(II)/TiO_2$ and $Pt(IV)/TiO_2$ samples. The XPS results show the photodeposition of Pt^{4+} ions onto the TiO_2 nanorod surfaces in an ethanol-containing aqueous solution resulted in the deposition of metallic Pt (or Pt(0)) on the brookite TiO_2 nanorod surface with a small proportion of PtO (or Pt(II)). The surface concentrations of Pt(0) and PtO were determined from the XPS spectrum to be 83.5% and 16.5%, respectively. In the $Pt(II)/TiO_2$ sample, Pt XPS spectrum indicate the presence of four types of Pt species on the TiO_2 nanorod surfaces: PtO, $[Pt(II)Cl_4]^{2-}$ (abbreviated as Pt(II)-Cl), PtO_2 and $[Pt(IV)Cl_6]^{2-}$ (abbreviated as Pt(IV)-Cl).[34] From the XPS spectrum, the surface concentrations of PtO, Pt(II)-Cl, PtO_2 and Pt(IV)-Cl were determined to be 39.7%, 23.3%, 10.0% and 27.1%, respectively. In the $Pt(IV)/TiO_2$ sample, the chemisorption of $[Pt(IV)Cl_6]^{2-}$ on the TiO_2 nanorod surfaces formed high concentration of PtO_2 (~79.4%) and some Pt(IV)-Cl (~20.6%). The chemisorption of $[Pt(II)Cl_4]^{2-}$ or $[Pt(IV)Cl_6]^{2-}$ onto TiO_2 nanoparticle surfaces is known to lead to the formation of covalently bounded surface complex.[35-37] Chloride substitution by surface $[Ti]\text{-}O^-$ is feasible, and in addition, very stable Ti–O–Pt bonds can be formed under ambient conditions.[37] Hence, PtO and PtO_2 are the associated chemisorbed products in the $Pt(II)/TiO_2$ sample while PtO_2 is a chemisorbed product in the $Pt(IV)/TiO_2$ sample.

Fig. S5, S6 and S7 (SI) shows the HRTEM images and EDX elemental mapping of $Pt(0)/TiO_2$, $Pt(II)/TiO_2$ and $Pt(IV)/TiO_2$ samples, respectively. The HRTEM image of $Pt(0)/TiO_2$ revealed the metallic Pt exists as small Pt nanoparticles with diameters in the range of 2-10 nm on the surfaces of the brookite TiO_2 nanorods. On the other hand, for the $Pt(II)/TiO_2$ and $Pt(IV)/TiO_2$ samples, the entire surfaces of the brookite TiO_2

nanorods were uniformly coated with a thin film layer of Pt(II) oxides or Pt(IV) oxides.

Scheme 2a shows the preparation steps of the Fe(II)-Pt(II)/TiO_2 samples. The brookite TiO_2 nanorods were initially dispersed and stirred in an aqueous solution containing only $[Pt(IV)Cl_6]^{2-}$ with nitrogen bubbling and sonication. Subsequently, UV photo-irradiation was provided while an aqueous Fe(II) sulfate solution was simultaneously injected into the Pt(IV)/TiO_2 powder-suspension to initiate the co-deposition of Pt and Fe sensitizers onto the TiO_2 nanorods.

Fig. S8a-d (SI) shows the XPS spectra of the Fe(III)-Pt(II)/TiO_2 sample. The Pt 4f XPS spectrum in Fig. S8d shows the presences of PtO (65.3%), Pt(II)-Cl (~18.1%) and PtO_2 (~16.6%). XPS peaks associated with Pt(IV)-Cl were not detected on the nanorod surfaces implying the $[Pt(IV)Cl_6]^{2-}$ on the TiO_2 surfaces had been photo-reduced to PtO and Pt(II)-Cl. The PtO_2 was likely formed from the subsequent oxidation of the PtO in ambient environment. The Fe 2p XPS spectrum in Fig. S8c indicates the presence of Fe oxide sensitizers with an oxidation state of +3 on the TiO_2 nanorod surface. The Fe(III) 2p3/2 at band energies of 710.0 eV and 712.2eV can be associated with nano-sized Fe_2O_3[38]and γ-FeOOH[39], respectively, suggesting that Fe(II) cations was oxidized to Fe(III) oxide nanoparticles by the photogenerated holes during the photodeposition process. Fe_2O_3 was the predominant species formed on the surface of the brookite TiO_2 nanorods with a small amount of γ-FeOOH. In addition, the formation of Fe_2O_3 and γ-FeOOH on the brookite TiO_2 nanorod surfaces can be further observed in an Fe 2p XPS spectrum when the photodeposition of the Fe(II) cations was conducted at higher precursor loading of 10wt% Fe(II), as shown in Fig. S9 (SI). At higher loading of Fe(III) oxides, the Fe_2O_3 and γ-FeOOH exhibit surface properties resembling that of Fe_2O_3 and γ-FeOOH bulk materials, as indicated by the Fe(III) 2p3/2 bands at higher binding energies of 710.7 eV and 712.1 eV, respectively.[40]

Overall, the XPS results show the photodeposition of $[Pt(IV)Cl_6]^{2-}$ on the brookite TiO_2 nanorod surfaces in the presence of Fe(II) cations led to the co-formation of Fe(III) oxide sensitizers and Pt(II)/(IV) sensitizers. In addition, it can be observed the concentration of Pt(II) sensitizers in the Fe(III)-Pt(II)/TiO_2 sample is significantly higher than that of the Pt(II)/TiO_2 sample. The Fe(III)-Pt(II)/TiO_2 sample contains 65.3% PtO and 18.1% Pt(II)-Cl, corresponding to a total Pt(II) concentration of 83.4%. On the other hand, the Pt(II)/TiO_2 sample, which contains 39.7 % PtO and 23.3% Pt(II)-Cl, has a lower total Pt(II) concentration of 63%. Hence, the merit of co-depositing Fe(III) oxide sensitizers with Pt sensitizers is that the Fe(III) oxides can limit the oxidation of the Pt(II) species (PtO and Pt(II)-Cl) to Pt(IV) species (PtO_2 and Pt(IV)-Cl), thereby stabilizing the Pt sensitizer oxidation state in a 2+ state. By contrast, if ethanol was used as the hole scavenger instead of Fe(II) cations, the Pt^{4+} ($[Pt(IV)Cl_6]^{2-}$) would be photoreduced to Pt(0) metal, as demonstrated by the Pt(0)/TiO_2 sample.

Fig. 1A-F shows HRTEM images and EDX (energy dispersive X-ray spectroscopy) elemental mapping of the as-prepared Fe(III)-Pt(II)/TiO_2 nanorods. The elemental mapping of the Fe(III)-Pt(II)/TiO_2 nanorods clearly showed the Pt(II) sensitizer was

selectively photo-deposited on the {210} facet of the brookite TiO_2 nanorods and accumulated in nanometer-sized island-like structures on the {210} facet. Unlike Pt(II) nanoparticles, the Fe(III) oxide sensitizer was not selectively photo-deposited on any particular facet of the brookite TiO_2 nanorods. Instead, the Fe(III) oxide sensitizer formed a uniform thin film layer coating on the entire Pt(II)/TiO_2 nanorods.

Fig. S2 (SI) also shows the XRD spectra of the Pt(0)/TiO_2, Pt(II)/TiO_2, Fe(III)/TiO_2 (prepared by chemisorption method) and Fe(III)-Pt(II)/TiO_2 sample. The XRD spectra indicate the modification of the as-prepared brookite TiO_2 with Pt/Fe sensitizers did not result in any XRD peak shift or the formation of new diffraction peaks belonging to metallic Pt or $Fe(OH)_3$. These observations suggest the Fe(III) and Pt sensitizers are not embedded into the bulk structures of brookite TiO_2 but are likely only deposited on the surfaces of the brookite TiO_2 nanorods.

2.2 Surface Affinities of Brookite TiO_2 for Fe^{2+}, Fe^{3+} and Pt^{4+} Cations

To elucidate how the Fe(III) oxide sensitizer layer was formed on the surfaces of the Pt(II)/TiO_2 nanorods upon photodeposition of Fe(II) and Pt(IV) ions , the surface adsorption capability of brookite TiO_2 nanorods for Fe(II), Fe(III) and Pt(IV) ions was investigated. Table S1 (SI) summarized the concentrations of Fe cations that were found deposited on the brookite TiO_2 samples after stirring the TiO_2 samples in known concentrations of Fe(II) or Fe(III)-containing solutions under dark conditions. The brookite TiO_2 nanorods could adsorb as much as 3.7wt% of Fe(III) cations when the brookite TiO_2 nanorods were stirred in in an Fe(III)-containing solution containing 4wt% Fe(III) cations. However, the brookite TiO_2 nanorods could only adsorb at maximum 0.23wt% of Fe(II) cations when the TiO_2 nanorods were stirred in a 4wt% Fe(II) solution. The results of ICP-MS show brookite TiO_2 exhibits high surface affinity for Fe(III) adsorption but low surface affinity for Fe(II) adsorption. The adsorption of Fe(II) and by TiO_2 was previously studied by Nano and Strathmann,[41] Zhang[42] and Hiemstra.[43] At the TiO_2 surface, the Fe^{2+} ion is presumably bound as a quattro-dentate surface complex ($\equiv(TiO)_2(TiOH)_2$-Fe(II)). This quattro-dentate surface complex exhibits high surface charge attribution with the TiO_2 surface.[42] Consequently, the hydrolysis and adsorption of Fe^{2+} on TiO_2 shows high pH dependency.[41] The adsorption of Fe(II) on TiO_2 is favored at pH>~7.5 (>80%) while significantly low at lower pH (<10%). In the current chemisorption conditions, the Fe(II) solution exhibits a pH of ~6 while the Fe(II)/Pt(IV) photo-deposition solution has a pH of ~3.8, th ese pH are relatively low for effective Fe(II) adsorption on TiO_2. In contrast, for Fe(III), the major Fe(III) species in solution at ~pH 3.5 are $[Fe(OH)(H_2O)_5]^{2+}$ and $[Fe(H_2O)_6]^{3+}$.[44] These hydrolyzed monomers can effectively adsorb onto TiO_2 surfaces.

The surface adsorption capability of brookite TiO_2 nanorods for Pt(IV) ions in the dark was also elucidated. The brookite TiO_2 nanorods exhibit high surface affinity for Pt(IV) ions. ICP results indicate that all of the Pt(IV) ions were adsorbed onto the brookite TiO_2 nanorod surfaces when the brookite TiO_2 nanorods were stirred in

aqueous solutions containing 0.1-0.6 wt% Pt(IV) in dark conditions, as shown in Table S2 (SI). As mentioned above, the chemisorption of $[Pt(IV)Cl_6]^{2-}$ onto TiO_2 surface forms a covalently bound surface complex by chloride substitution at the surface [Ti]-O^-. Under ambient conditions, these Pt(IV)-Cl surface complexes are partly converted to highly stable Ti-O-Pt bonds.[45]

The results of ICP-MS show for the TiO_2 nanorod sample co-deposited with Fe(II) and Pt(IV) ions, both at nominal loadings of 0.4wt%, only 0.07wt% of Fe(II) cations in the aqueous solution was eventually deposited on the TiO_2 nanorod surfaces to form the Fe(III) oxide thin film sensitizer coating (see Table S2). On the other hand, for Pt, all of the 0.4wt% of Pt(IV) ions in the solution were adsorbed onto the TiO_2 nanorod surfaces.

2.3 Proposed Formation Mechanism of Fe(III)- Pt(II)/TiO_2 Nanorods

Scheme 2b shows the proposed formation mechanism of Fe(III)-Pt(II)/TiO_2 nanorods. The $[Pt(IV)Cl_6]^{2-}$ were reduced by the photogenerated electrons of TiO_2 to form Pt(II) nanoparticles (i.e., PtO, Pt(II)-Cl) on the brookite TiO_2 nanorod surfaces. Attributed to the low surface affinity of the brookite TiO_2 nanorods for Fe(II) cations, as revealed by ICP-MS and discussed above, the brookite TiO_2 nanorod surfaces contained only small amounts of surface-adsorbed Fe(II) cations. Consequently, when the surface-adsorbed Fe(II) cations on the TiO_2 nanorods were oxidized by the photogenerated holes, the Fe(II) cations formed a very thin layer of the Fe(III) oxide sensitizer (i.e., Fe_2O_3/FeOOH) on the entire surfaces of the Pt(II)-sensitized TiO_2 nanorods. Notably, the presence of the Fe(III) oxide thin film sensitization layer inhibits further reduction of the Pt(II) to Pt(IV) species, resulting in the formation of significantly high surface concentrations of Pt(II) sensitizers on the TiO_2 nanorod surfaces (~83.4%). Since TiO_2 is a demonstrated water oxidation photocatalyst, the electron used for the oxidation of Fe(II) and the reduction of Pt(IV) during the photo-deposition reaction is balanced by a concurrent oxidation of water.[46]

2.4 Optical Properties

Optical properties of the as-prepared brookite TiO_2 photocatalysts were elucidated using UV-Vis spectra. Fig. 2A shows the UV-Vis diffuse absorption spectra of pure brookite TiO_2, Fe(III)/TiO_2, Pt(II)/TiO_2 and Fe(III)-Pt(II)/TiO_2. Pure brookite TiO_2 shows an absorption edge at 380 nm, corresponding to an optical band gap of ~3.3 eV. Owing to the photo-sensitizing effects of the Fe(III) and Pt(II)/(IV) sensitizers, the brookite TiO_2 nanorod samples exhibit visible light absorption tails in the wavelength region of 400-600 nm upon surface modifications with the Fe and/or Pt sensitizers.[47, 48] The visible light absorption tail is observed to be stronger for the Pt(II)/TiO_2 sample than for the Fe(III)/TiO_2 sample. This observation indicates the Pt(II)/(IV)sensitizers have greater visible light responses than that of the Fe(III) oxide sensitizers suggesting that Pt(II)/(IV) sensitizers are likely to be better visible light-driven sensitizers than

Fe(III) oxide sensitizers. For the Fe(III)-Pt(II)/TiO_2 nanorod sample, the co-loading of Pt(II) and Fe(III) oxide sensitizers onto brookite TiO_2 nanorods results in the most apparent red shift in the visible light absorption. Since the Fe(III)-Pt(II)/TiO_2 nanorod sample contains higher concentrations of Pt(II) sensitizers and lower concentration of Pt(IV) sensitizers compared to that of the Pt(II)/TiO_2 sample, the enhanced visible light absorption property of Fe(III)-Pt(II)/TiO_2 nanorod sample can be attributed to the Pt(II) sensitizers.

2.5 Photocatalytic Activities of Fe(III) and Pt-sensitized TiO_2 and Fe(III)-Pt(II)-oxide-co-sensitized TiO_2 nanorods

The activities of as-prepared brookite TiO_2 nanorods and Fe(III) or Pt-sensitized brookite TiO_2 nanorod samples for photocatalytic degradation of acetaldehyde under visible light illumination were investigated. Prior to the light irradiation, the samples were investigated under dark conditions. Fig. S10 shows the CO_2 concentration-time profiles of the samples upon exposure to acetaldehyde under dark conditions. In all samples, low concentrations of CO_2 (~20-50 ppm) were detected within 30 min exposure to acetaldehyde and the CO_2 levels remained unchanged therefore. Since adsorbed CO_2 are naturally present on a TiO_2 oxide surface, the detection of CO_2 under dark conditions suggests there is a surface-exchange of CO_2 for acetaldehyde on the TiO_2 surfaces.[49-51] That is, adsorbed CO_2 desorbed from the TiO_2 surfaces upon exposure to acetaldehyde and acetaldehyde was re-adsorbed onto the TiO_2 surfaces. It is energetically infeasible for pure TiO_2 or the Pt/Fe-sensitized TiO_2 to degrade acetaldehyde spontaneously under dark conditions and evolve CO_2, particularly at CO_2 levels of ~20-50 ppm within 30 min.[49]

For all samples, the CO_2 concentration generated from photocatalytic acetaldehyde degradation is determined after subtracting the amount of CO_2 that were desorbed under dark conditions (abbreviated as ΔCO_2). Fig. S11 (SI) shows the concentrations of CO_2 generated from acetaldehyde degradation when Pt(II)/TiO_2 and Fe(III)/TiO_2 with varied nominal loading of Pt sensitizers or Fe(III) oxide sensitizer were utilized as the photocatalysts. For both Pt(II)/TiO_2 and Fe(III)/TiO_2, the photocatalytic activities increased with increase in the weight loading of Pt sensitizers or Fe(III) oxide sensitizers until an optimum concentration was derived, whereby the photocatalytic activity was highest. A further increase in concentrations of Pt or Fe(III) sensitizers resulted in a decrease in activities, probably due to an excessive coverage of Pt or Fe(III) sensitizers on the active sites of TiO_2, which hinders efficient transport of photoexcited electrons. The optimum weight loading of Pt sensitizers and Fe(III) oxide sensitizers on brookite TiO_2 for photocatalytic degradation of acetaldehyde were both found to be at a nominal loading of 0.4wt% Fe or Pt. While the actual loading of Pt in the optimal Pt(II)/TiO_2 sample is also 0.4wt% due to the high surface affinity of brookite TiO_2 for Pt ions, the actual loading of Fe element in the optimal Fe(III)/TiO_2 sample is 0.23% (see Table S3). Hence, for the co-deposition of Pt(IV) ions and Fe(II) cations on

brookite TiO_2 nanorods to form an Fe(III)-Pt(II)/TiO_2 photocatalyst, nominal loading of 0.4wt% was applied for both Fe(II) and Pt(IV).

Fig. 2B shows the CO_2 concentrations from photocatalytic degradation of acetaldehyde over Fe(III)-Pt(II)/TiO_2, Fe(III)/TiO_2 and pure brookite TiO_2 photocatalysts. The Fe(III)-Pt(II)/TiO_2 photocatalyst shows the highest activity among the three samples. In a 5-h photocatalytic test, Fe(III)-Pt(II)/TiO_2 generated more than 300 ppm of CO_2, which is approximately two-times higher than that generated by Fe(III)/TiO_2(<100 ppm CO_2). The pure brookite TiO_2 photocatalyst shows some visible light activity, it generated minor amount of CO_2 in 5h (~16.5 ppm CO_2). The Ti XPS spectrum of pure brookite TiO_2 nanorods, Fig. S12, indicate the presence of low concentration of Ti^{3+} defect states on the surface of the brookite TiO_2 nanorods. The visible light activity of the brookite TiO_2 can be attributed to the visible light absorption at the Ti^{3+} defect centers. Low concentrations of oxygen vacancies are commonly observed in TiO_2 nanorods due to the ease of formation of oxygen vacancies in TiO_2 nanostructures.[52, 53] Fig. 2C and D show the action spectra of Fe(III)-Pt(II)/TiO_2 and pure TiO_2 samples. The wavelength-dependent action spectra of Fe(III)-Pt(II)/TiO_2 indicate the apparent quantum efficiencies (AQE) of the Fe(III)-Pt(II)/TiO_2 photocatalyst and pure TiO_2 match well with their UV-Vis absorbance. The dependence of photocatalytic activities with different wavelengths of light indicate the light absorption by the Fe(III)-Pt(II)/TiO_2 and pure TiO_2 photocatalysts is the main factor contributing to the photocatalytic reactions. The Fe(III)-Pt(II)/TiO_2 photocatalyst exhibited an AQE of 0.84% under 420 nm monochromatic light irradiation. It should be noted the BET surface area analyses show the as-prepared brookite TiO_2 nanorods with and without modifications with Fe and/or Pt sensitizers exhibit equivalent surface areas of ~54-56 m^2/g. The BET surface areas of as-prepared TiO_2 samples are summarized in Table S3 (SI).

2.6 Photocatalytic Activities of Pt(0) and Pt(II) and Pt(IV) Sensitizer-modified Brookite TiO_2 Nanorods

In order to investigate the activities and stabilities of Pt sensitizers with different oxidation states for photocatalytic degradation of acetaldehyde under visible light, photocatalytic tests were conducted for Pt(0)/TiO_2, Pt(II)/TiO_2, Pt(IV)/TiO_2 and Fe(III)-Pt(II)/TiO_2 over three repeated cycles. Fig. 3 shows the CO_2 concentrations produced from the photocatalytic degradation of acetaldehyde over Pt(0)/TiO_2, Pt(II)/TiO_2, Pt(IV)/TiO_2 and Fe(III)-Pt(II)/TiO_2. Among the Pt-sensitized TiO_2 samples (without Fe(III) co-loading), Pt(II)/TiO_2 shows the highest photocatalytic activity. When Pt(II)/TiO_2 was used, 250 ppm of CO_2 was generated from the degradation of acetaldehyde in the first photocatalytic cycle of 5 h. In contrast, <100 ppm and <90 ppm of CO_2 were generated in the first cycle tests with Pt(IV)/TiO_2 and Pt(0)/TiO_2, respectively. Although Pt(II)/TiO_2 shows the highest activity for photocatalytic degradation of acetaldehyde in the first 5-h cycle, the Pt(II)/TiO_2 sample shows poor stability on subsequent 5-h cycles. The CO_2 concentrations generated in the second and

third 5-h cycles decreased to 76% and 50%, respectively, of the concentration in the first cycle. On the other hand, the Pt(IV)/TiO_2 and Pt(0)/TiO_2 samples show strong stability with no deterioration in activities over the three 5-h cycles.

To elucidate the structural change in Pt(II)/TiO_2 after photocatalytic tests leading to the decreased activities, the Pt(II)/TiO_2 sample was investigated by XPS before and after a photocatalytic test. Fig. 4 shows the Pt 4f XPS spectra of a fresh Pt(II)/TiO_2 sample and a spent Pt(II)/TiO_2 sample that was photo-irradiated in acetaldehyde under visible light for 24 h. As aforementioned, the as-prepared Pt(II)/TiO_2 sample consists of PtO (39.7%), Pt(II)-Cl (23.3%), PtO_2 (10.0%) and Pt(IV)-Cl (27.1%). After the 24-h photocatalytic reaction with acetaldehyde, the XPS results of the spent Pt(II)/TiO_2 sample, as can be seen in Fig. 4B, show significant reductions in peak intensities for PtO and Pt(II)-Cl. On the other hand, the peak intensities for PtO_2 and Pt(IV)-Cl showed significant increased. The Pt compositions in the spent Pt(II)/TiO_2 sample are as follows: PtO (20.7%), Pt(II)-Cl (12.3%), PtO_2 (29.6%) and Pt(IV)-Cl (37.4%) Hence, the reduced photocatalytic activity of the Pt(II)/TiO_2 sample can be attributed to the oxidation of PtO and Pt(II)-Cl to PtO_2 and Pt(IV)-Cl, respectively. The results imply the Pt(II) sensitizers are more effective visible light sensitizers than the Pt(IV) sensitizers, albeit with lower stability.

The optical properties of a Pt(II)/TiO_2 sample before and after the 24-h photocatalytic reaction with acetaldehyde as well as those of a fresh Pt(IV)/TiO_2 sample were also measured by UV-Vis spectroscopy. UV-Vis diffuse absorption spectra of these samples are shown in Fig. S13 and S14 (SI). The as-prepared Pt(II)/TiO_2 shows a stronger visible light absorption tail in the 400-600 nm wavelength region compared to the as-prepared Pt(IV)/TiO_2 sample. After the 24-h photocatalytic test, the UV-Vis spectra of the post-treated Pt(II)/TiO_2 sample shows a reduction in visible light absorption intensity in the 400-600 nm wavelength region. Hence, the decrease in photocatalytic activities of the Pt(II)/TiO_2 sample in the repeated photocatalytic tests can be attributed to a reduced ability of the Pt(II)/TiO_2 sample to absorb visible light due to an increased conversion of Pt(II) to Pt(IV) during the photocatalytic degradation process.

2.7 Importance of Fe(III) Oxide Sensitizer Outer Layer for Enhancing the Photocatalytic Activity and Stability of Pt(II)/TiO_2

Fig. 3 also shows the CO_2 concentration from photocatalytic degradation of acetaldehyde over the Fe(III)-Pt(II)/TiO_2 photocatalyst. It is notable that the co-modifications of the Fe(III) and Pt(II) sensitizers on the brookite TiO_2 nanorods improved not only the photocatalytic activity of Pt(II)/TiO_2 but also the cycling stability of the sample. The Fe(III)-Pt(II)/TiO_2 photocatalyst generated 325 ppm of CO_2 for all three 5-h cycles with no deterioration, which is a significant enhancement compared to the 250 ppm of CO_2 generated by Pt(II)/TiO_2 in the first cycle (Fig. 3). Fig. S15 shows the cycling stability test for Fe(III)/TiO_2. Similar to Fe(III)-Pt(II)/TiO_2 photocatalyst, the Fe(III)/TiO_2 shows stability for photocatalytic acetaldehyde degradation over three

5-h cycles, it generated ~100-110 ppm of CO_2 in each cycle. XPS was also utilized to examine the Fe(III)-Pt(II)/TiO_2 photocatalyst after 24-h photocatalytic degradation of acetaldehyde. Fig. 4C and D show the Pt spectra of the Fe(III)-Pt(II)/TiO_2 sample before and after the photocatalytic test. The XPS indicate an increased in PtO concentration in the spent- Fe(III)-Pt(II)/TiO_2 sample (from 65.3% in the fresh sample to 77.8% in the spent sample). On the other hand, the concentrations of Pt(II)-Cl and PtO_2 showed reductions in the spent sample. The Pt(II)-Cl and PtO_2 in the fresh Fe(III)-Pt(II)/TiO_2 sample were 18.1% and 16.6%, respectively, while 15.3% and 5.1% in the spent Fe(III)-Pt(II)/TiO_2 sample, respectively. The increased in PtO concentration accompanied with concurrent reductions of Pt(II)-Cl and PtO_2 concentrations in the spent Fe(III)-Pt(II)/TiO_2 sample indicate some of the PtO_2 were photoreduced to PtO while some of the Pt(II)-Cl were also converted to PtO during the photocatalytic degradation of acetaldehyde. It is energetically feasible for the Cl^- ligands to form free Cl^- radicals during the photocatalytic oxidation reactions.[45, 54, 55]

2.8 Direct Visualization of Electron Transfer in Fe/Pt-sensitized TiO_2 Nanorods under Visible Light Irradiation using *in situ* DB-PAS

In order to elucidate the electron transfer mechanisms of Fe/Pt-sensitized TiO_2 leading to the obtained activities, the behaviors of injected electrons in pure brookite TiO_2 and Fe/Pt-sensitized TiO_2 were investigated by *in situ* DB-PAS. Fig. 5A shows the time-course curves of PA intensity under visible light irradiation in the presence of air and 2-PrOH vapor for pure brookite TiO_2, Fe(III)/TiO_2, Pt(II)/TiO_2 and Fe(III)-Pt(II)/TiO_2. The PA intensity increased upon visible light irradiation because Ti(IV) was reduced to Ti(III) by the injected electrons from the loaded metal cations into TiO_2. However, the number of electrons accumulated in the TiO_2 by visible light irradiation was much smaller, compared to the maximum capacity of electron accumulation in the TiO_2. The steady-state values of PA intensity show dependence on the kind of metal oxide sensitizer(s) loaded onto TiO_2 in the order of Fe(III)-Pt(II)/TiO_2 > Pt(II)/TiO_2 > Fe(III)/TiO_2 > TiO_2. Because these measurements were carried out in the presence of an electron acceptor such as O_2, the PA intensity is related to the difference between the amount of injected electrons and electrons consumed on TiO_2. Previous studies show some metal oxide compounds function as not only visible light sensitizers but also electron acceptor.[56] Therefore, it is difficult to estimate the amount of electron injection only from PA intensity measured in the presence of O_2. However, the almost same increases in PA intensity for Fe(III)-Pt(II)/TiO_2 and Pt(II)/TiO_2 under visible light irradiation indicate that electron consumption was hardly changed by the co-loading of Fe(III) oxides on Pt(II)/TiO_2. Overall, the PA intensities indicate Pt(II) oxide works as a more efficient visible light sensitizer than Fe(III) oxide sensitizer, in good agreement with the UV-Vis light absorption spectra (Fig. 2A). By contrast, the Fe(III)/TiO_2 showed a lower PA intensity than the Pt(II)/TiO_2 or the Fe(III)-Pt(II)/TiO_2 because the amount of injected electrons from the Fe(III)/TiO_2 was much smaller due to the lower photoabsorption of the Fe(III)/TiO_2.

Fig. 5B shows time-course curves of PA intensity for Fe(III)-Pt(II)/TiO_2 and Pt(II)/TiO_2 under visible light irradiation in artificial air only. The PA intensity for both samples increased under visible light irradiation even in the absence of electron donor, i.e., 2-PrOH vapor. However, the PA intensity of Pt(II)/TiO_2 decreased after prolonged light irradiation, indicating the efficiency of electron injection was decreased in the absence of 2-PrOH electron donor. The decrease in PA intensity is likely to be due to the self-oxidation of Pt(II) to Pt(IV), as indicated by XPS results (Fig. 4) and UV-Vis spectra (Fig. S13 and S14, SI). In contrast, the PA intensity for Fe(III)-Pt(II)/TiO_2 increased under prolonged light irradiation even in the absence of 2-PrOH electron donor. This observation is presumably because the co-loaded Fe(III) oxide sensitizer retards the self-oxidation of Pt(II) oxide sensitizer and the rate of electron injection from Pt(II) stabilized by Fe(III) is continuously faster than that of electron consumption.

2.9 Proposed Mechanisms of Photocatalytic Acetaldehyde Degradation over Pt(II)/TiO_2 and Fe(III)-Pt(II)/TiO_2 under Visible Light

The proposed mechanisms for acetaldehyde degradation over Pt(II)/TiO_2 and Fe(III)-Pt(II)/TiO_2 photocatalyts under visible light is presented in Fig. 6A. For Pt(II)/TiO_2, upon visible light photoexcitation of the Pt(II) oxide sensitizer, photoexcited electrons are transferred from the Pt(II) oxide sensitizer to the conduction band of TiO_2 and O_2 is reduced to superoxide radicals ($O_2^{\cdot-}$) at the TiO_2 surface active sites. Simultaneously, the photoexcited holes oxidize acetaldehyde to CO_2 at the Pt(II) oxide sensitizer photocatalytic sites. However, the oxygen in the air can also extract electrons from the Pt(II) oxide sensitizer and directly oxidize Pt(II) to Pt(IV). The decrease in the concentration of the Pt(II) oxide sensitizer in the Pt(II)/TiO_2 sample with time reduces both the light absorption ability and photocatalytic activity of the Pt(II)/TiO_2 photocatalyst.

In the case of the Fe(III)-Pt(II)/TiO_2 photocatalyst, upon photoexcitation of both Fe(III) and Pt(II) oxide sensitizers with visible light, photocatalytic degradation of acetaldehyde occurs on both the Fe(III) and Pt(II) oxide sensitizers. The Fe(III) oxide sensitizer protective layer around the Pt(II)/TiO_2 nanorods can protect the Pt(II) oxide sensitizer from oxidation by continuously injecting its photoexcited electrons into the Pt(II) oxide sensitizer, as evidenced by the *in situ* DB-PAS, leading to enhanced photocatalytic activity and sustained stability.

In addition, the electron injected into the conduction band of TiO_2 is expected to reduce O_2 to superoxide anions ($\bullet O_2^-$), which is further reduced into hydrogen peroxide (H_2O_2) and hydroxyl (OH) radicals by subsequent second and third electron transfer, respectively,[23, 57, 58] as shown in Fig. 6A. As the H_2O_2 and OH radicals have high oxidizing powers,[59] they will be consumed in the oxidation reaction of acetaldehyde.

Besides the direct experimental evidence from *in situ* DB-PAS, the first principle DFT calculations also support the proposed charge transfer mechanisms. Since PtO and Fe_2O_3 are the dominant components of Pt(II) and Fe(III) oxide sensitizers, we modeled

the heterojunction interface of PtO and Fe_2O_3 and that of PtO and brookite TiO_2. The obtained electron density distribution maps are presented in Figure 6B. The electron density distribution map of the Fe_2O_3 and PtO heterojunction interface indicates electrons are accumulating at the PtO sites, suggesting that electrons are spontaneously transferring from Fe_2O_3 to PtO. On the other hand, at the heterojunction interface of PtO and TiO_2, electrons are accumulating at the TiO_2 sites, suggesting that electrons are migrating spontaneously from PtO to TiO_2. Taken together, the favorable tri-component interfaces of Fe_2O_3/PtO/TiO_2 allow rapid transfer of photoexcited electrons from Fe_2O_3 to PtO and then to TiO_2, where the electrons are eventually scavenged by ambient O_2 at the TiO_2 surface. The rapid removal of photoexcited electrons from Fe_2O_3 and PtO also extends the lifetime of photoexcited holes at the Fe_2O_3 and PtO surfaces, which in turn enhances the hole oxidation reaction of acetaldehyde to CO_2 at the Fe(III) and Pt(II) oxide photocatalytic sites.

3. Conclusions

In summary, single-crystalline brookite TiO_2 nanorods with well-defined {210} and {111} facets were successfully fabricated by a hydrothermal process using TALH as a shaping agent. Among the Pt sensitizers of different oxidation states, Pt(II) oxide-sensitized TiO_2 shows the highest photocatalytic activity for degradation of acetaldehyde under visible light. However, the stability of Pt(II) oxide is compromised by its self-oxidation to Pt(IV) during the photocatalytic reaction with acetaldehyde. Surface coating of a Fe(III) oxide sensitizer thin film layer around the Pt(II)/TiO_2 nanorods can prevent the self-oxidation of Pt(II) oxide sensitizer through electron injection, enabling enhanced stability and enhanced activity. The energetically favorable tri-component interfaces of Fe_2O_3/PtO/TiO_2 allow photoexcited electrons to migrate rapidly from the outermost Fe(III) oxide sensitizer to the mid-zone Pt(II) oxide sensitizer and then to TiO_2. The enhanced separation of electrons and holes promotes the hole oxidation reaction of acetaldehyde at the Fe(III) and Pt(II) oxide photocatalytic sites. The Fe(III)-Pt(II)/TiO_2 photocatalyst exhibited an AQE of 0.84% under 420 nm monochromatic light irradiation for acetaldehyde degradation, which is significantly higher than that of pure brookite TiO_2 (0.14%)**.**

Supporting Information.

The Supporting Information is available free of charge.

Experimental section and additional characterization data and activity tests of as-prepared brookite TiO_2 nanorods and Fe/Pt sensitized TiO_2 nanorods (XRD, Raman Spectrum, HRTEM and SAED pattern, XPS, UV-vis diffuse spectra and BET surface area).

Acknowledgements

The authors acknowledge the financial support of JSPS, Grant-in-Aid for Scientific Research (B) (20H02847), National Natural Science Foundation of China

(21805191), the Guangdong Basic and Applied Basic Research Foundation (2020A1515010982), Shenzhen Stable Support Project (20200812122947002) and Brain Pool Program through the National Research Foundation of Korea (NRF) funded by the Ministry of Science and ICT (Brain Pool Program Grant Number: 2019H1D3A1A01070035). The authors thank Dr. Nan Jian from the Electron Microscope Center of the Shenzhen University for his help in HRTEM measurement.

References

[1] Z.N. Tong, Discussion on the health problems of indoor living, IOP Conference Series: Earth and Environmental Science, 186 (2018).

[2] C. Guo, Z. Gao, J. Shen, Emission rates of indoor ozone emission devices: A literature review, Building and Environment, 158 (2019) 302-318.

[3] P. Harb, N. Locoge, F. Thevenet, Treatment of household product emissions in indoor air: Real scale assessment of the removal processes, Chemical Engineering Journal, 380 (2020).

[4] Y.-J. Hu, L.-J. Bao, C.-L. Huang, S.-M. Li, P. Liu, E.Y. Zeng, Exposure to air particulate matter with a case study in Guangzhou: Is indoor environment a safe haven in China?, Atmospheric Environment, 191 (2018) 351-359.

[5] H. Salonen, T. Salthammer, L. Morawska, Human exposure to NO_2 in school and office indoor environments, Environ Int, 130 (2019) 104887.

[6] R.M. Alberici., W.F. Jardim, Photocatalytic destruction of VOCs in the gas-phase using titanium dioxide, Applied Catalysis B: Environmental, 14 (1997) 55-68.

[7] M. Meisutovic-Akhtarieva, T. Prasauskas, D. Ciuzas, E. Krugly, K. Keraityte, D. Martuzevicius, V. Kauneliene, Impacts of exhaled aerosol from the usage of the tobacco heating system to indoor air quality: A chamber study, Chemosphere, 223 (2019) 474-482.

[8] M. Salaspuro, Key role of local acetaldehyde in upper GI tract carcinogenesis, Best Pract Res Clin Gastroenterol, 31 (2017) 491-499.

[9] X. Zhang, J. Cao, J. Wei, Y. Zhang, Improved C-history method for rapidly and accurately measuring the characteristic parameters of formaldehyde/VOCs emitted from building materials, Building and Environment, 143 (2018) 570-578.

[10] T. Fukumura, E. Sambandan, H. Yamashita, Synthesis and VOC degradation ability of a CeO_2 /WO_3 thin-layer visible-light photocatalyst, Materials Research Bulletin, 94 (2017) 493-499.

[11] S. Song, C. Lu, X. Wu, S. Jiang, C. Sun, Z. Le, Strong base g-C3N4 with perfect structure for photocatalytically eliminating formaldehyde under visible-light irradiation, Applied Catalysis B: Environmental, 227 (2018) 145-152.

[12] A. Enesca, Y. Yamaguchi, C. Terashima, A. Fujishima, K. Nakata, A. Duta, Enhanced UV–Vis photocatalytic performance of the $CuInS_2$ /TiO_2 /SnO_2 hetero-structure for air decontamination, Journal of Catalysis, 350 (2017) 174-181.

[13] R. Yang, Q. Chen, Y. Ma, R. Zhu, Y. Fan, J. Huang, H. Niu, Y. Dong, D. Li, Y. Zhang, L. Mei, B. Chen, Z. Zeng, Highly efficient photocatalytic hydrogen evolution and simultaneous formaldehyde degradation over Z-scheme ZnIn2S4-NiO/BiVO4 hierarchical heterojunction under visible light irradiation, Chemical Engineering Journal, 423 (2021).

[14] Y. Peng, S. Kang, Z. Hu, Pt Nanoparticle-Decorated CdS Photocalysts for CO2 Reduction and H2 Evolution, ACS Applied Nano Materials, 3 (2020) 8632-8639.

[15] S. Song, Z. Sheng, Y. Liu, H. Wang, Z. Wu, Influences of pH value in deposition-precipitation synthesis process on Pt-doped TiO2 catalysts for photocatalytic oxidation of NO, Journal of Environmental Sciences, 24 (2012) 1519-1524.
[16] M. Yoshida., A. Yamakata., K. Takanabe., J. Kubota., M. Osawa., K. Domen, ATR-SEIRAS Investigation of the Fermi Level of Pt Cocatalyst on a GaN Photocatalyst for Hydrogen Evolution under Irradiation, Journal of the American Chemical Society, 131 (2009) 13218-13219.
[17] Y. Hu, X. Song, S. Jiang, C. Wei, Enhanced photocatalytic activity of Pt-doped TiO_2 for NOx oxidation both under UV and visible light irradiation: A synergistic effect of lattice Pt^{4+} and surface PtO, Chemical Engineering Journal, 274 (2015) 102-112.
[18] C.-H. Huang, I.K. Wang, Y.-M. Lin, Y.-H. Tseng, C.-M. Lu, Visible light photocatalytic degradation of nitric oxides on PtOx-modified TiO_2 via sol-gel and impregnation method, Journal of Molecular Catalysis A: Chemical, 316 (2010) 163-170.
[19] F. Dong, H. Wang, G. Sen, Z. Wu, S.C. Lee, Enhanced visible light photocatalytic activity of novel Pt/C-doped TiO_2/$PtCl_4$ three-component nanojunction system for degradation of toluene in air, J Hazard Mater, 187 (2011) 509-516.
[20] M. Nishikawa, H. Sakamoto, Y. Nosaka, Reinvestigation of the photocatalytic reaction mechanism for Pt-complex-modified TiO_2 under visible light irradiation by means of ESR spectroscopy and chemiluminescence photometry, J Phys Chem A, 116 (2012) 9674-9679.
[21] C. Wang, H. Fan, X. Ren, Y. Wen, W. Wang, Highly dispersed PtO nanodots as efficient co-catalyst for photocatalytic hydrogen evolution, Applied Surface Science, 462 (2018) 423-431.
[22] M. Sansotera, S. Geran Malek Kheyli, A. Baggioli, C.L. Bianchi, M.P. Pedeferri, M.V. Diamanti, W. Navarrini, Absorption and photocatalytic degradation of VOCs by perfluorinated ionomeric coating with TiO2 nanopowders for air purification, Chemical Engineering Journal, 361 (2019) 885-896.
[23] Q. Zeng, X. Wang, X. Xie, G. Lu, Y. Wang, S. Cheng Lee, J. Sun, TiO_2/TaS_2 with superior charge separation and adsorptive capacity to the photodegradation of gaseous acetaldehyde, Chemical Engineering Journal, 379 (2020).
[24] J.J.M. Vequizo, H. Matsunaga, T. Ishiku, S. Kamimura, T. Ohno, A. Yamakata, Trapping-Induced Enhancement of Photocatalytic Activity on Brookite TiO2 Powders: Comparison with Anatase and Rutile TiO_2 Powders, ACS Catalysis, 7 (2017) 2644-2651.
[25] H.T.T. Tran, H. Kosslick, M.F. Ibad, C. Fischer, U. Bentrup, T.H. Vuong, L.Q. Nguyen, A. Schulz, Photocatalytic Performance of Highly Active Brookite in the Degradation of Hazardous Organic Compounds Compared to Anatase and Rutile, Applied Catalysis B: Environmental, 200 (2017) 647-658.
[26] W.-K. Li., X.-Q. Gong., G. Lu., A. Selloni., Different Reactivities of TiO_2 Polymorphs: Comparative DFT Calculations of Water and Formic Acid Adsorption at Anatase and Brookite TiO_2 Surfaces, The Journal of Physical Chemistry C, 112 (2008) 6594-6596.
[27] Z. Li, S. Cong, Y. Xu, Brookite vs Anatase TiO2 in the Photocatalytic Activity for Organic Degradation in Water, ACS Catalysis, 4 (2014) 3273-3280.
[28] M. Addamo, M. Bellardita, A. Di Paola, L. Palmisano, Preparation and photoactivity of nanostructured anatase, rutile and brookite TiO_2 thin films, Chem Commun (Camb), (2006) 4943-4945.
[29] J. Zhang, S. Yan, L. Fu, F. Wang, M. Yuan, G. Luo, Q. Xu, X. Wang, C. Li, Photocatalytic Degradation of Rhodamine B on Anatase, Rutile, and Brookite TiO_2, Chinese Journal of Catalysis, 32 (2011) 983-991.
[30] X.-Q. Gong, A. Selloni, First-principles study of the structures and energetics of stoichiometric

brookiteTiO2surfaces, Physical Review B, 76 (2007).
[31] T. Ohno, T. Higo, H. Saito, S. Yuajn, Z. Jin, Y. Yang, T. Tsubota, Dependence of photocatalytic activity on aspect ratio of a brookite TiO_2 nanorod and drastic improvement in visible light responsibility of a brookite TiO_2 nanorod by site-selective modification of Fe^{3+} on exposed faces, Journal of Molecular Catalysis A: Chemical, 396 (2015) 261-267.
[32] J. Jin, J. Luo, L. Zan, T. Peng, One-Pot Synthesis of Cu-Nanocluster-Decorated Brookite TiO_2 Quasi-Nanocubes for Enhanced Activity and Selectivity of CO_2 Photoreduction to CH_4, Chemphyschem, 18 (2017) 3230-3239.
[33] I.A. Mkhalid, J.L.G. Fierro, R.M. Mohamed, A.A. Alshahri, Visible light driven photooxidation of imazapyr herbicide over highly efficient mesoporous $Ag/Ag_2O–TiO_2$ p-n heterojunction photocatalysts, Ceramics International, 46 (2020) 25822-25832.
[34] A. Romanchenko, M. Likhatski, Y. Mikhlin, X-ray Photoelectron Spectroscopy (XPS) Study of the Products Formed on Sulfide Minerals Upon the Interaction with Aqueous Platinum (IV) Chloride Complexes, Minerals, 8 (2018).
[35] Burgeth. G, K. H, Photocatalytic and photoelectrochemical properties of titania/ chloroplatinate(IV), Coordination Chemistry Reviews, 230 (2002) 41-47.

[36] W. Macyk, K. Szaciłowski, G. Stochel, M. Buchalska, J. Kuncewicz, P. Łabuz, Titanium(IV) complexes as direct TiO2 photosensitizers, Coordination Chemistry Reviews, 254 (2010) 2687-2701.
[37] Macyk. W, K. H, Photosensitization of Crystalline and Amorphous Titanium Dioxide by Platinum (IV) Chloride Surface Complexes, Chemistry-A European Journal, 7 (2001) 1862-1867.
[38] A.P. Grosvenor, B.A. Kobe, M.C. Biesinger, N.S. McIntyre, Investigation of multiplet splitting of Fe 2p XPS spectra and bonding in iron compounds, Surface and Interface Analysis, 36 (2004) 1564-1574.
[39] L. Shen, Y. Cao, Z. Du, W. Zhao, K. Lin, L. Jiang, Illuminate the active sites of γ-FeOOH for low-temperature desulfurization, Applied Surface Science, 425 (2017) 212-219.
[40] X.-q. Li, W.-x. Zhang, Iron Nanoparticles: the Core-Shell Structure and Unique Properties for Ni(II) Sequestration, Langmuir, 22 (2006) 4638-4642.
[41] G.V. Nano, T.J. Strathmann, Ferrous iron sorption by hydrous metal oxides, J Colloid Interface Sci, 297 (2006) 443-454.
[42] Z. Zhang, P. Fenter, L. Cheng, N. C. Sturchio, M. J. Bedzyk, M. Pr˘edota, A. Bandura, J. D. Kubicki, S. N. Lvov, P. T. Cummings, A. A. Chialvo, M. K. Ridley, P. Be´ne´zeth, L. Anovitz, D.A. Palmer, M. L. Machesky, a.D.J. Wesolowski, Ion Adsorption at the Rutile-Water Interface: Linking Molecular and Macroscopic Properties, Langmuir, 20 (2004) 4954-4969.

[43] T. Hiemstra, W.H. van Riemsdijk, Adsorption and surface oxidation of Fe(II) on metal (hydr)oxides, Geochimica et Cosmochimica Acta, 71 (2007) 5913-5933.
[44] E. Piera, M.I. Tejedor-Tejedor, M.E. Zorn, M.A. Anderson, Relationship concerning the nature and concentration of Fe(III) species on the surface of TiO2 particles and photocatalytic activity of the catalyst, Applied Catalysis B: Environmental, 46 (2003) 671-685.
[45] F.J. Gracia, J.T. Miller, A.J. Kropf, E.E. Wolf, Kinetics, FTIR, and Controlled Atmosphere EXAFS Study of the Effect of Chlorine on Pt-Supported Catalysts during Oxidation Reactions, Journal of Catalysis, 209 (2002) 341-354.
[46] H. Eidsvag, S. Bentouba, P. Vajeeston, S. Yohi, D. Velauthapillai, TiO_2 as a Photocatalyst for Water Splitting-An Experimental and Theoretical Review, Molecules, 26 (2021).

[47] Huogen Yu, Hiroshi Irie, Yoshiki Shimodaira, Yasuhiro Hosogi, Yasushi Kuroda, Masahiro Miyauchi, K. Hashimoto, An Efficient Visible-Light-Sensitive Fe(III)-Grafted TiO2 Photocatalyst, J. Phys. Chem. C, 114 (2010) 16481-16487.
[48] Jina Choi, Hyunwoong Park, M.R. Hoffmann, Effects of Single Metal-Ion Doping on the Visible-Light Photoreactivity of TiO_2, J. Phys. Chem. C, 114 (2010) 783-792.
[49] Alexis Markovits, Adil Fahmi, C. Minot, A theoretical study of CO_2 adsorption on TiO_2, Journal of Molecular Structure (Theochem), 371 (1996) 219-235.
[50] Y.-H. Lin, C.-H. Weng, J.-H. Tzeng, Y.-T. Lin, Adsorption and Photocatalytic Kinetics of Visible-Light Response N-Doped TiO_2 Nanocatalyst for Indoor Acetaldehyde Removal under Dark and Light Conditions, International Journal of Photoenergy, 2016 (2016) 1-9.
[51] Y. Ma, Q. Tang, W.-Y. Sun, Z.-Y. Yao, W. Zhu, T. Li, J. Wang, Assembling ultrafine TiO_2 nanoparticles on UiO-66 octahedrons to promote selective photocatalytic conversion of CO_2 to CH_4 at a low concentration, Applied Catalysis B: Environmental, 270 (2020).
[52] Fan Zuo, Le Wang, Tao Wu, Zhenyu Zhang, Dan Borchardt, P. Feng, Self-Doped Ti^{3+} Enhanced Photocatalyst for Hydrogen Production under Visible Light, J. Am. Chem. Soc., 132 (2010) 11856–11857.
[53] X. Wang, Y. Li, X. Liu, S. Gao, B. Huang, Y. Dai, Preparation of Ti^{3+} self-doped TiO2 nanoparticles and their visible light photocatalytic activity, Chinese Journal of Catalysis, 36 (2015) 389-399.
[54] G. I. STRAGUZZI, H. R. ADURIZ, C.E. GIGOLA, Redispersion of Platinum on Alumina Support, JOURNAL OF CATALYSIS, 66 (1980) 171-183.
[55] E. Marceau, H. Lauron-Pernot, M. Che, Influence of the Metallic Precursor and of the Catalytic Reaction on the Activity and Evolution of Pt(Cl)/δ-Al2O3 Catalysts in the Total Oxidation of Methane, Journal of Catalysis, 197 (2001) 394-405.
[56] T. Ohno., D. Haga., K. Fujihara., K. Kaizaki., M. Matsumura., Unique Effects of Iron(III) Ions on Photocatalytic and Photoelectrochemical Properties of Titanium Dioxide, The Journal of Physical Chemistry B, 101 (1997) 6415-6419.
[57] T. Hirakawa, K. Yawata, Y. Nosaka, Photocatalytic reactivity for O_2^- and OH radical formation in anatase and rutile TiO_2 suspension as the effect of H_2O_2 addition, Applied Catalysis A: General, 325 (2007) 105-111.
[58] H. Kim, W. Choi, Effects of surface fluorination of TiO_2 on photocatalytic oxidation of gaseous acetaldehyde, Applied Catalysis B: Environmental, 69 (2007) 127-132.
[59] J.-H. Xu, F. Shiraishi, Photocatalytic decomposition of acetaldehyde in air over titanium dioxide, Journal of Chemical Technology and Biotechnology, 74 (1999) 1096-1100.

FIGURES

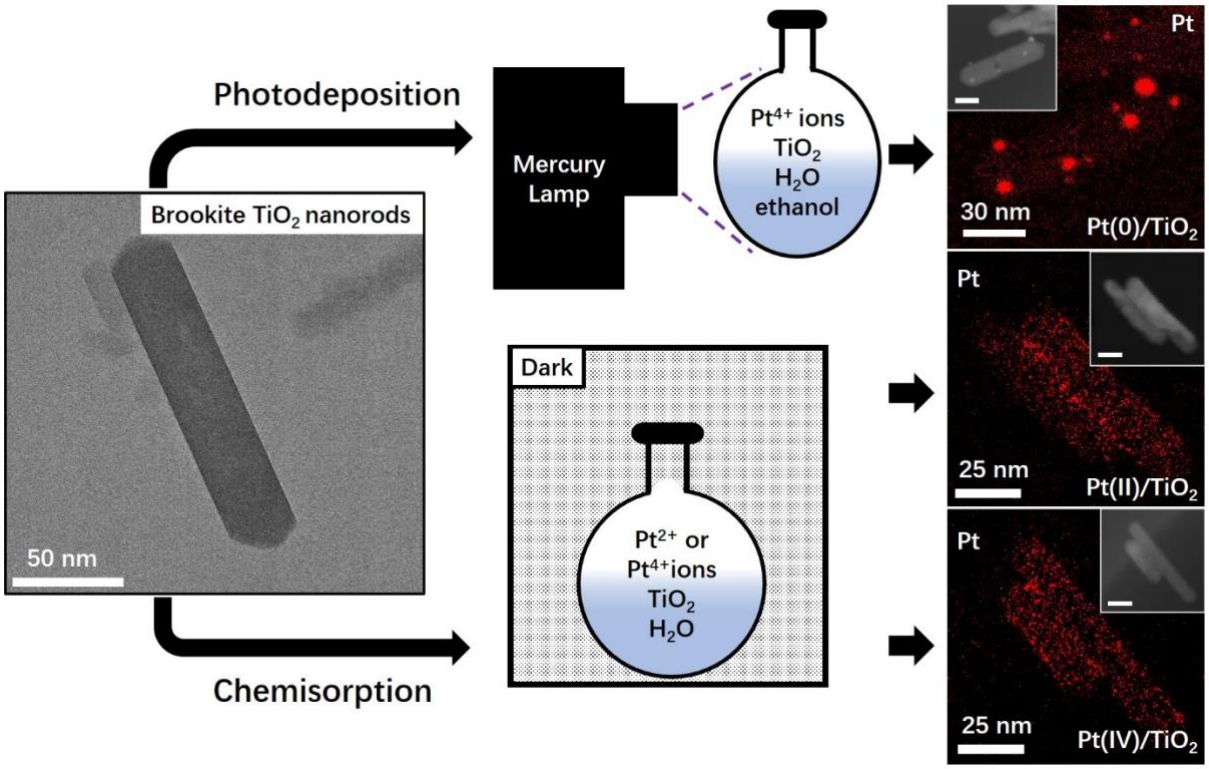

Scheme 1. A material flowchart showing the synthesis of metallic Pt-sensitized brookite TiO_2 nanorods (Pt(0)/TiO_2) by a photo-deposition method and, Pt(II) oxide-sensitized brookite TiO_2 nanorods (Pt(II)/TiO_2) and Pt(IV) oxide-sensitized brookite TiO_2 nanorods (Pt(VI)/TiO_2) by a chemisorption method. Scale bar in inset for Pt(0)/TiO_2 represents 30 nm and 25 nm for Pt(II)/TiO_2 and Pt(IV)/TiO_2. The Pt TEM-EDX spectrum and HRTEM image (inset) of a Pt(0)/TiO_2 sample showed the metallic Pt exists as small Pt nanoparticles with diameters in the range of 2-10 nm on the surfaces of the brookite TiO_2 nanorods. On the other hand, for Pt(II)/TiO_2 and Pt(IV)/TiO_2 samples, the entire surfaces of the brookite TiO_2 nanorods were uniformly coated with a thin film layer of Pt(II) oxides or Pt(IV) oxides.

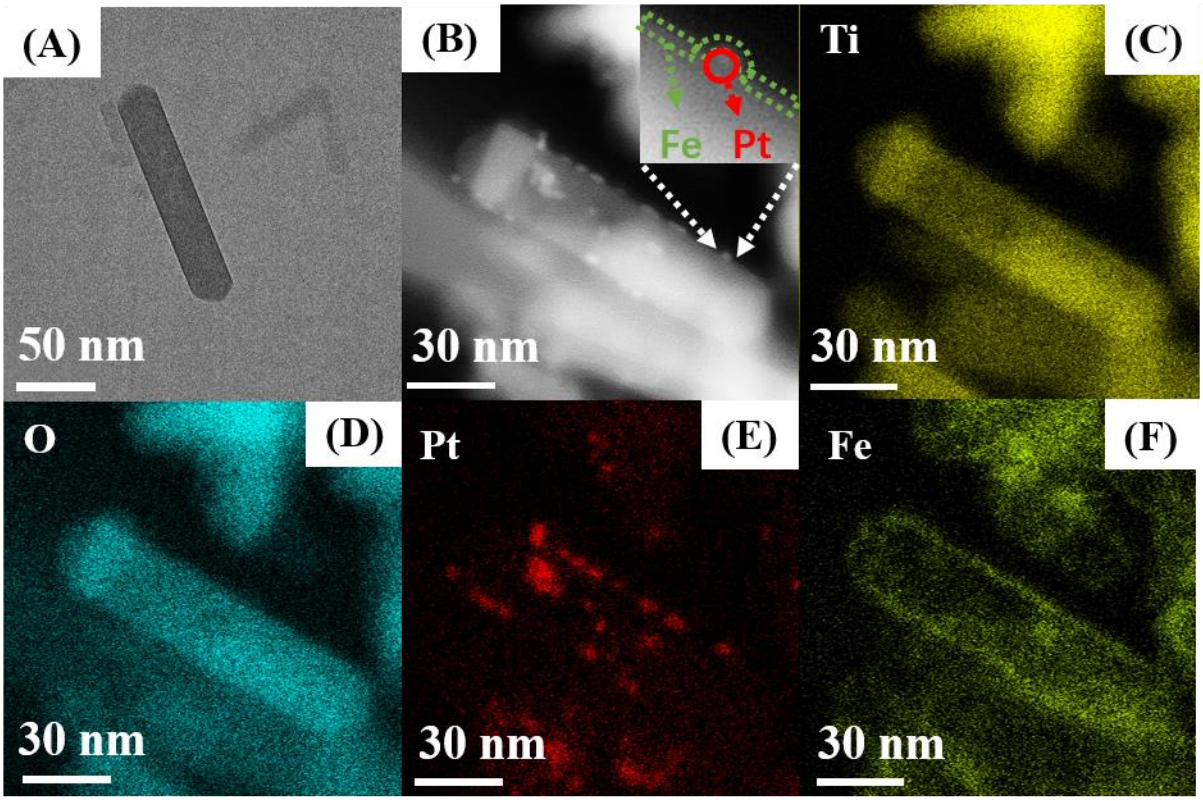

Figure 1. HRTEM images of (A) pure brookite TiO_2 nanorods and (B) Fe(III)-Pt(II)-oxide-co-sensitized brookite TiO_2 nanorods (B) and the associated EDX elemental mapping of the as-prepared Fe(III)-Pt(II)-oxide-co-sensitized brookite TiO_2 nanorods (C) Ti, (D) O, (E) Pt and (F) Fe.

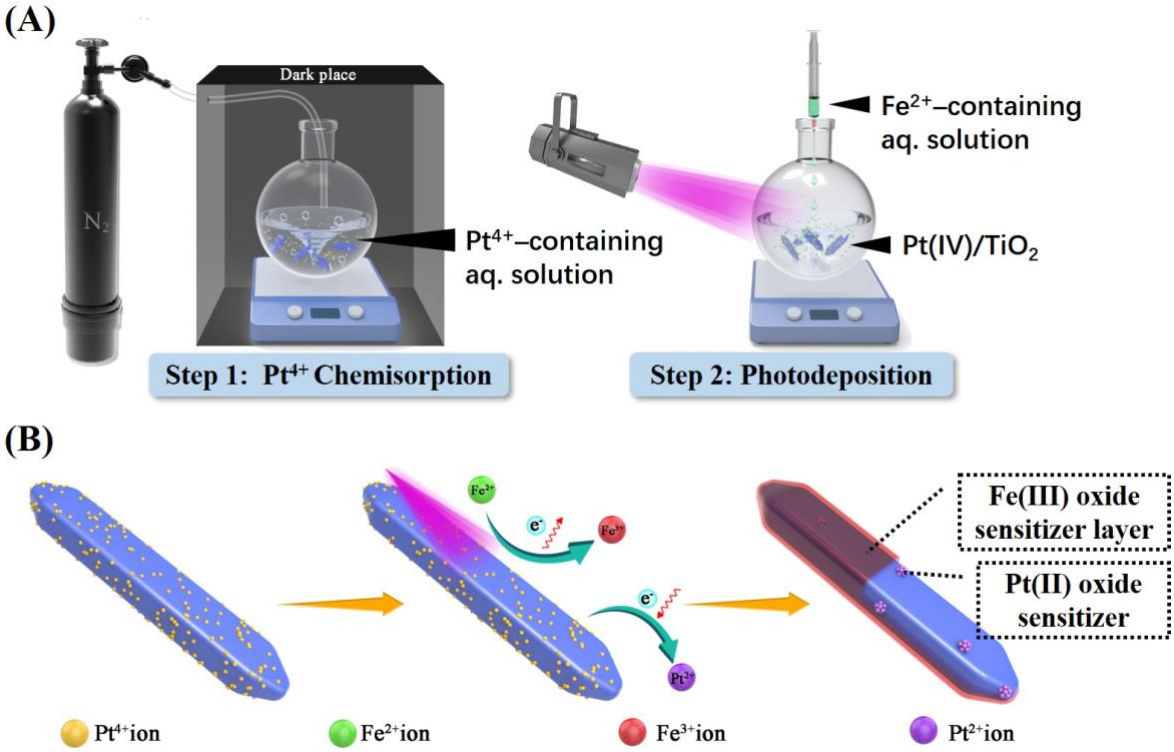

Scheme 2. (A) The preparation steps of Fe(III)-Pt(II)-oxide-co-sensitized brookite TiO_2 nanorods (Fe(II)-Pt(II)/TiO_2). Pt^{4+} cations were first chemisorbed onto the brookite TiO_2 nanorods under dark conditions and anoxic conditions. Subsequently, an aqueous solution of Fe(II) sulfate was injected into the Pt^{4+}-containing solution upon light-irradiation and the co-photodeposition of Pt^{4+} and Fe^{2+} cations onto the brookite TiO_2 nanorods occurred to form Fe(III)-Pt(II)/TiO_2 nanorods. **(B)** Proposed formation mechanism of Fe(III)-Pt(II)/TiO_2 nanorods. The chemisorbed Pt^{4+} cations on the TiO_2 nanorod surfaces were reduced by the photogenerated electrons of TiO_2 to form Pt(II) oxide nanoparticles on the brookite TiO_2 nanorod surfaces. Owing to the low surface affinity of the brookite TiO_2 nanorods for Fe(II) cations, the brookite TiO_2 nanorod surfaces contained low concentration of surface-adsorbed Fe(II) cations, which were subsequently oxidized by the photogenerated holes of TiO_2 to form a very thin layer of the Fe(III) oxide sensitizer over the entire surfaces of the Pt(II) oxide-sensitized TiO_2 nanorods.

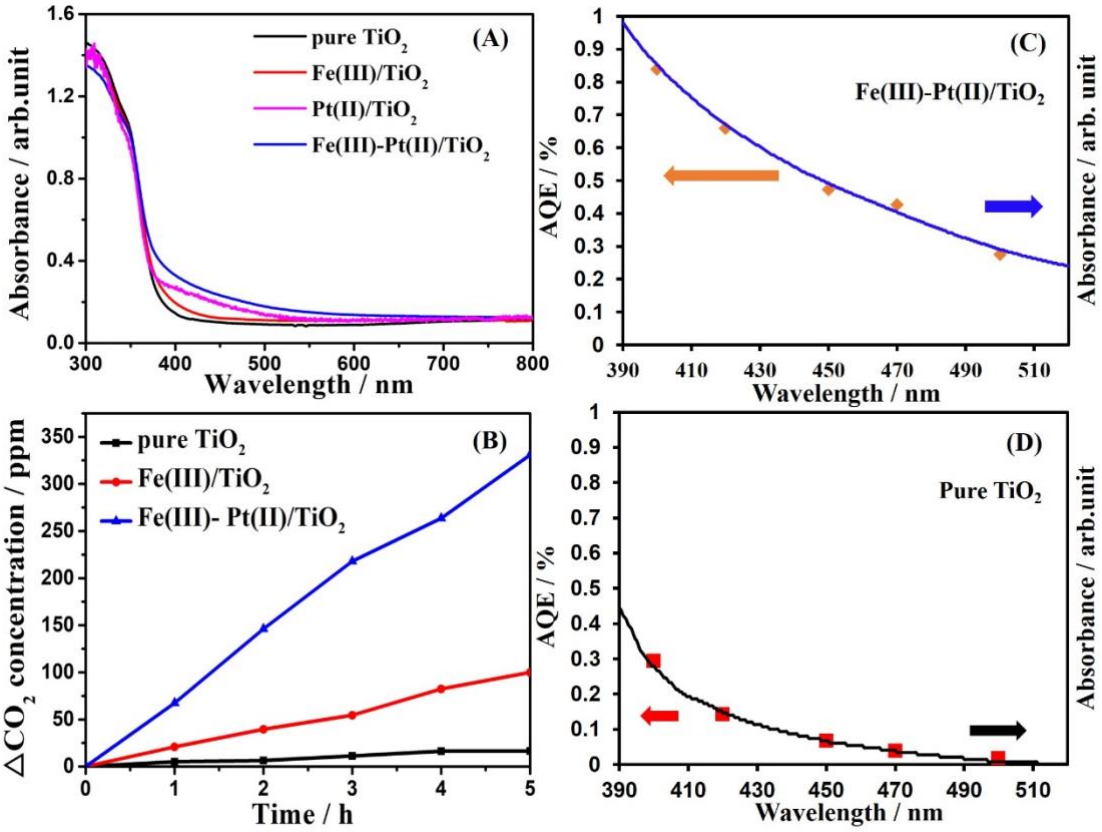

Figure 2. (A) UV-Vis diffuse absorption spectra of pure brookite TiO_2, Fe(III)/TiO_2, Pt(II)/TiO_2 and Fe(III)-Pt(II)/TiO_2 samples, (B) CO_2 concentrations generated from photocatalytic degradation of acetaldehyde under visible light using Fe(III)-Pt(II)/TiO_2, Fe(III)/TiO_2 and pure brookite TiO_2 photocatalysts and, wavelength-dependent action spectrum of (C) Fe(III)-Pt(II)/TiO_2 and (D)pure TiO_2.

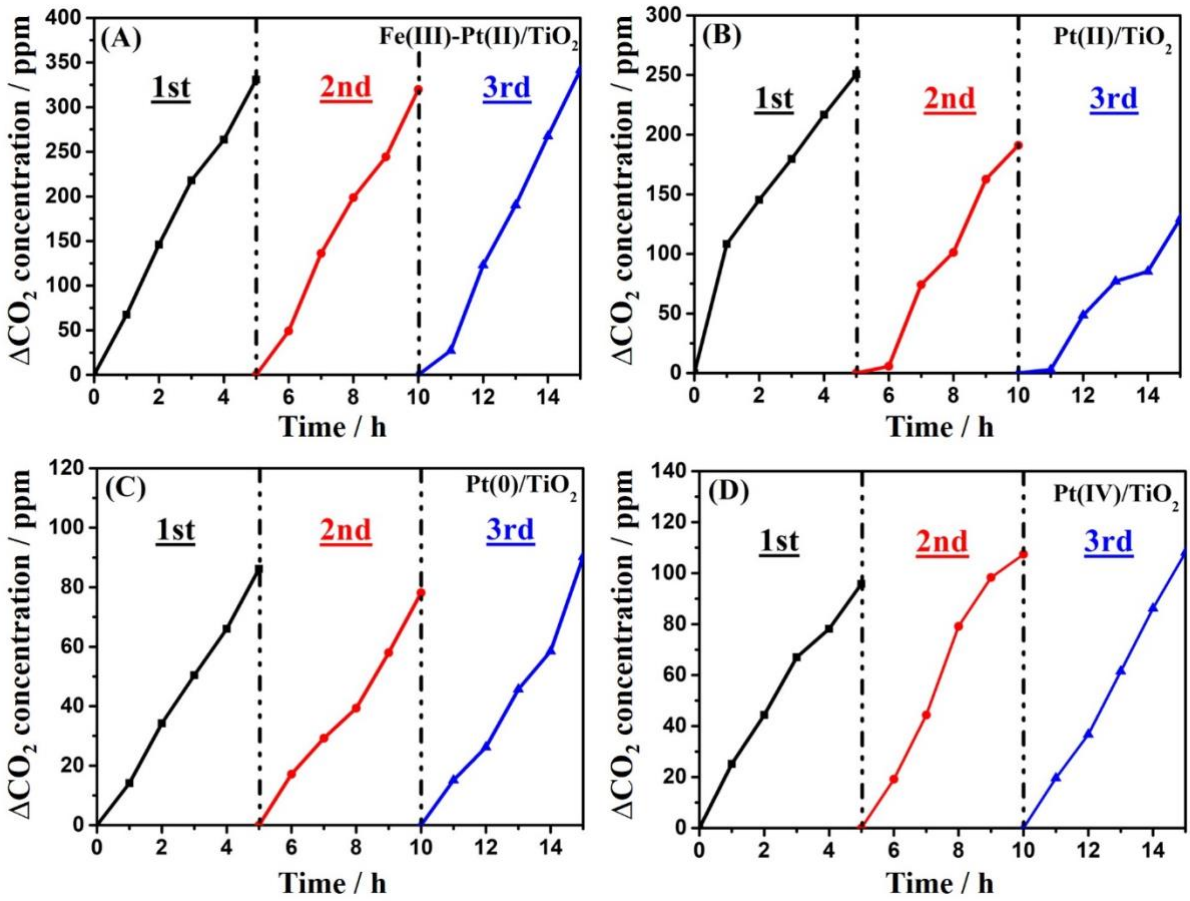

Figure 3. CO_2 concentrations generated from the photocatalytic degradation of acetaldehyde under visible light using (A) Fe(III)-Pt(II)/TiO_2, (B) Pt(II)/TiO_2, (C) Pt(0)/TiO_2, and (D) Pt(IV)/TiO_2 samples. All samples contained 0.4wt% Pt. Fe(III)-Pt(II)/TiO_2 contained 0.07 wt%Fe.

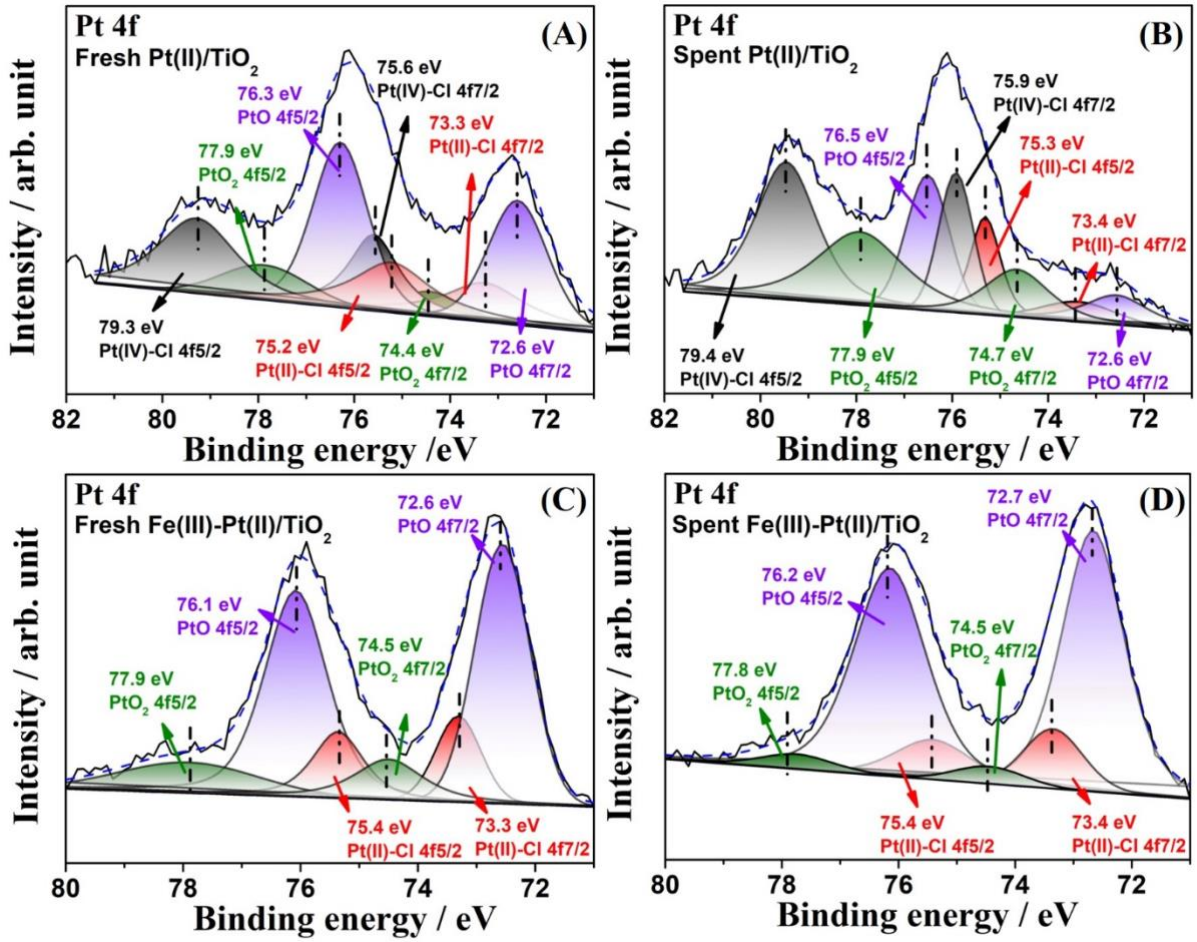

Figure 4. Pt 4f XPS spectra of a fresh Pt(II)/TiO_2 sample (A), a spent Pt(II)/TiO_2 sample that was photo-irradiated in acetaldehyde for 24 h (B), a fresh Fe(III)-Pt(II)/TiO_2 sample (C) and a spent Fe(III)-Pt(II)/TiO_2 sample (D) that was photo-irradiated in acetaldehyde for 24 h.

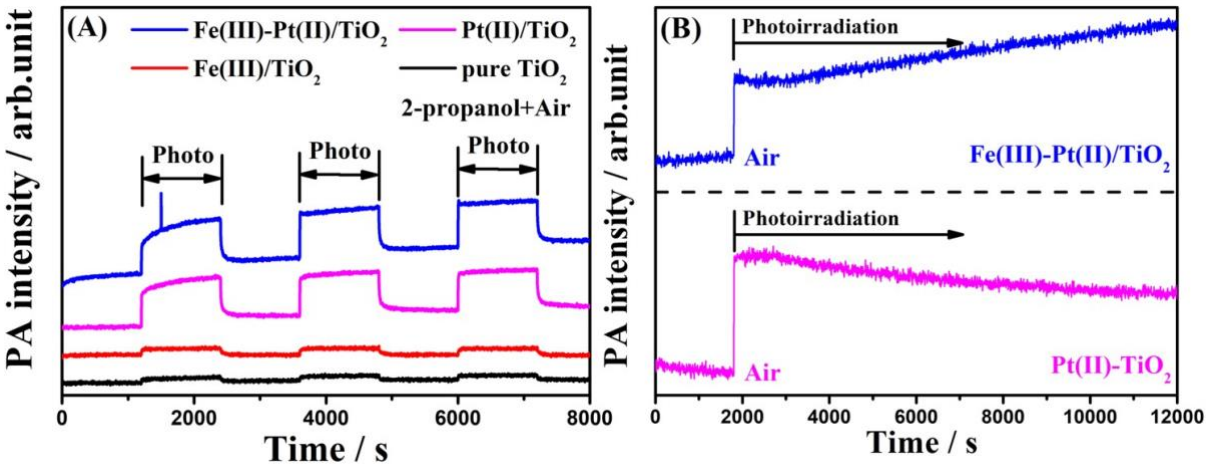

Figure 5. (A) The time-course curves of the PA intensity under intermittent visible light irradiation in the presence of air and 2-PrOH vapor for pure brookite TiO_2, Fe(III)/TiO_2, Pt(II)/TiO_2 and Fe(III)-Pt(II)/TiO_2 samples and (B) the time-course curves of the PA intensity under continuous visible light irradiation in the presence of air for Pt(II)/TiO_2 and Fe(III)-Pt(II)/TiO_2 samples.

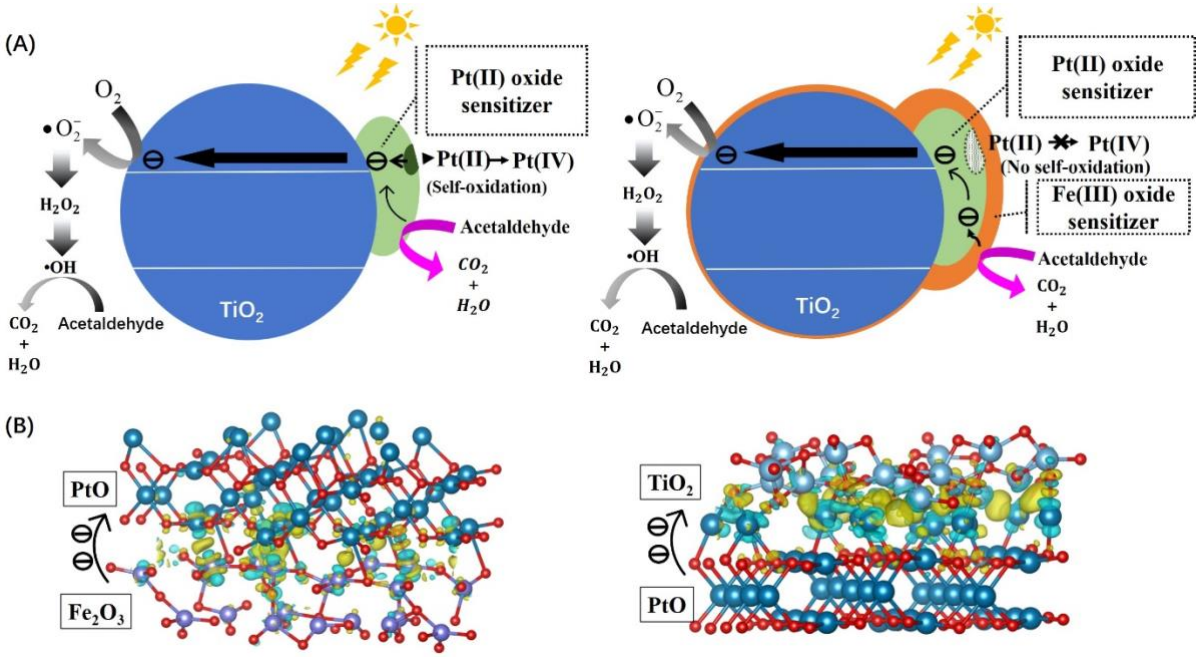

Figure 6. (A) Proposed mechanisms for acetaldehyde degradation over Pt(II)/TiO_2 and Fe(III)-Pt(II)/TiO_2 photocatalyts under visible light and (B) electron density distribution maps of PtO and brookite TiO_2 (left) and Fe_2O_3 and PtO heterojunction interfaces (right), color of spheres: red = O, dark blue = Pt, light blue = Ti and purple = Fe, yellow and green areas represent higher and lower electron density.